IEEE Access
Multidisciplinary ⋮ Rapid Review ⋮ Open Access Journal

Received 25 July 2023, accepted 7 August 2023, date of publication 22 August 2023, date of current version 30 August 2023.

Digital Object Identifier 10.1109/ACCESS.2023.3307388

RESEARCH ARTICLE

Using Dielectric Rods to Reconfigure Combline Filters in Center Frequency and Bandwidth

ABHISHEK SHARMA, (Student Member, IEEE), SANTIAGO COGOLLOS, (Member, IEEE), VICENTE E. BORIA, (Fellow, IEEE), AND MARCO GUGLIELMI, (Life Fellow, IEEE)
Instituto de Telecomunicaciones y Aplicaciones Multimedia (ITEAM), Universitat Politècnica de València, 46022 Valencia, Spain

Corresponding author: Abhishek Sharma (asharma@iteam.upv.es)

This work was supported in part by the European Union's Horizon 2020 Research and Innovation Program through the Marie Skłodowska-Curie Innovative Training Networks (ITN) (TESLA) under Grant 811232; and in part by the Minsiterio de Ciencia e Innovación (MICIN), Spanish Government, through the Research and Development Project under Grant PID2019-103982RB-C41 (funded by MICIN/AEI/10.13039/501100011033).

ABSTRACT This article describes the use of dielectric rods to reconfigure combline filters both with respect to center frequency and bandwidth. In this context, a new filter topology is developed in order to maximize the achievable reconfiguration range. The design of a prototype is discussed in detail, clearly demonstrating the feasibility of center frequency and bandwidth reconfiguration, with the same filter structure, while maintaining an equiripple return loss. In addition to theory, a combline filter prototype is also fabricated, tuned and measured in several configurations showing excellent agreement with simulations, thereby fully validating both the basic concept and the design procedure.

INDEX TERMS Band-pass filter, combline filters, dielectric tuners, reconfigurability, tunable filters.

I. INTRODUCTION

The current evolution trend in communication equipment requirements, for both ground and space applications, is towards an ever increasing use of bandwidth. However, the total available bandwidth is limited, so that the frequency spectrum that is allocated to each application is now fully regulated at world wide level [1]. To meet this challenge, modern communication systems are currently being developed with the ability of providing multi-channel communication systems, where each channel uses different center frequency and bandwidth [2].

In this context therefore, the possibility of developing microwave components, and filters in particular, that are agile in frequency has recently become a very important area of research [3], [4], [5]. Filters (and multiplexers) have always been considered key components for the front-end of communication equipment for both ground and space applications [6]. As a consequence, a very significant research effort has been devoted in the last decade to the development of filters and multiplexers that can be reconfigured both in terms of center frequency and bandwidth [7], [8].

The simplest approach to change the center frequency of a filter structure based on coupled cavities, is to change the size of the cavities. A number of different approaches that explore this possibility have indeed been reported in the technical literature. For instance, a compressible bellow or a conductive elastomer lid on the top of two dual-mode cavities has been demonstrated in [9]. A different concept has also been proposed in [10] discussing a contact-less corrugated plunger. Furthermore, one more approach is presented in [11], where the cavity size is changed by activating or deactivating an array of conductive lines located on the cavity wall. An additional approach has also been introduced in [12], for the reconfiguration of both center frequency and bandwidth by moving, at the same time, both end walls of a cylindrical cavity. Two more contributions can also be found in the technical literature, where the filter tunability is obtained by rotating a specially designed piece of dielectric material that is located inside the resonant cavities of the filter [13], [14].

Furthermore, in [15] a copper coated polyflon sheet is used to cover the top of a metallic cavity, and a piezoelectric

The associate editor coordinating the review of this manuscript and approving it for publication was Ye Zhou.

actuator is used to modify the cavity dimensions. Another approach is described in [16], where tuning disks are actuated using thermal MEMS. Several papers have also discussed capacitive coupling between resonator and tuning discs or posts. In [17] and [18], for instance, a floating capacitance between the disk and the post is modified using a MEMS-based capacitance or a varactor. One more approach is described in [19] where GaAs and MEMS capacitors are proposed. In [20], another tuning solution is adopted, namely, a varactor diode connected to the open end of a coaxial post resonator.

Another very common approach to tune filters based on waveguide cavities is to use metallic tuning elements or screws. This approach has been demonstrated with directly-coupled rectangular waveguide filters [21], and dual-mode filters [22]. Classical combline filter topologies can also be tuned with metallic screws, as it is shown in [23] and [24]. More recently, metal screws have also been used within re-entrant coaxial resonators, for tuning the frequency response while keeping the bandwidth constant [25]. However, the use of metallic tuning elements (or screws) for remotely reconfigurable filter implementations, can introduce a number of complications, namely:

- The tuning element or screw must be securely fastened to the filter body in order to operate correctly.
- The penetration of the tuning screw must be controlled very accurately to ensure the correct filter performance.
- The presence of metallic tuning elements may have a negative effect on the high power and passive intermodulation (PIM) performance of the filter.

Alternative solutions, based on the use of a single rotating mechanism driving all metal tuning elements, have been recently developed for E-plane filters [26], and coaxial filters [27]. These solutions have a simplified mechanical assembly, and also allow to keep a constant bandwidth in the achievable frequency tuning ranges. This is achieved using a clever design for the coupling elements of the filter. However, these new topologies can only produce filters with fixed bandwidth (approximately 2%), with a return loss of 15 dB.

In addition to metallic tuners, however, dielectric tuners have also been used more recently to tune microwave filters. In [28] and [29], their potential use for tuning standard rectangular waveguide filters is validated through full-wave simulations and measurements. A very recent work on the practical demonstration of dielectric tuners in inductive waveguide filters is discussed in [30]. It is important to note, at this point, that the results discussed in [30] are only applicable to rectangular waveguide filters based on *distributed* resonators. The present work, in contrast, intends to demonstrates the use of dielectric tuners in combline filters, where the resonators can essentially be considered as *lumped-element* resonators. In the context of combline filters, dielectric tuners were first used within resonators, in [31] and [32], for implementing tunable filters in terms of center frequency only (keeping constant the filter bandwidth). Additional initial results for the same tunable responses (only in terms of center frequency) have also been discussed in [33], where dielectric tuners are used in coupling windows to preserve the same filter bandwidth.

In this context, therefore, the objective of this paper is to significantly extend the initial results presented in [33]. The additional novel material discussed in this paper is as follows:

- In addition to Alumina, we also study the use of Zirconia, and we compare the key performance of the two dielectric materials.
- A new filter structure is then designed to take advantage of the superior performance of Zirconia.
- Furthermore, we show that both simulation and measurements indicate that Zirconia has a good quality factor, that is comparable to other established topologies using either metallic or dielectric tuners.
- In addition to changing the center frequency, we show how the same structure can also be used to change the bandwidth of the filter. In particular, we show that the combline filter can be reconfigured to maintain a constant absolute bandwidth throughout the frequency tuning range. Alternatively, the bandwidth of the filter can be increased up to twice the initial value.
- We show that the relation between the variation of the penetration of the tuning elements and the filter center frequency remains approximately linear. As a consequence, the prediction of the filter center frequency is greatly simplified.
- We discuss how the use of dielectric tuners eliminates the need for keeping a very good electrical contact with the body of the filter, thereby eliminating a common source of insertion loss and PIM.
- In addition to simulations, we also show the measured results of a prototype built using Zirconia, and we demonstrate successfully how the same filter structure can be reconfigured both in terms of center frequency and bandwidth.
- Furthermore, we show how the out of band performance of tunable filter can be improved with the integration of a simple lowpass filter. In this context, we also discuss the achievable improvements and limitations of this approach.
- In addition, we also study the high power behavior of our tunable filter, and discuss the possible trade-offs between power handling and tuning range.
- Finally, we discuss how the structure we propose opens the possibility of using low-accuracy, computer-controlled actuators to implement remotely controlled reconfiguration of the filter.

This article is organized as follows: In section II, the design of a frequency-tunable filter using dielectric rods made of Alumina is discussed in detail. We then discuss in section III the use of Zirconia as an alternative dielectric material, and derive a new set of initial filter dimensions. After that, we discuss in section IV the complete design of a filter that can be tuned both in terms of frequency and bandwidth.

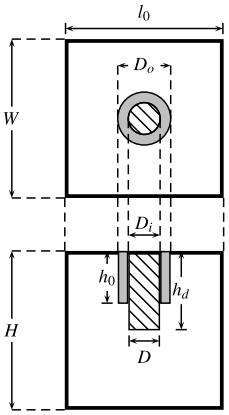

FIGURE 1. Cavity configuration where the dielectric tuner is inserted in the hollow post (top view and side view [33]).

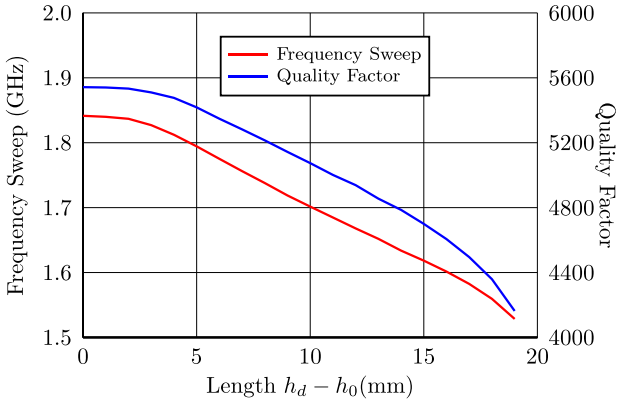

FIGURE 2. Frequency tuning range (left side scale) and Q_u factor (right side scale) provided by the structure in Fig. 1 as a function of the length of the dielectric rod exceeding the hollow post ($h_d - h_0$).

The details in the manufacturing process and the measured results are shown in sections V. In Section VI we discuss how the out-of-band response of the reconfigurable filter can be controlled. In Section VII we study the multipactor behavior of our filter. Section VIII describes the remote operation of the reconfigurable filter prototype. Finally, Section IX concludes the paper with a summary of the results achieved.

II. FREQUENCY-TUNABLE FILTER WITH ALUMINA DIELECTRIC TUNERS

In this section, we briefly recall, for the sake of completeness, the design of the frequency tunable filter based on Alumina tuners already discussed in [33], providing, at the same time, new information concerning the dimensions of the structure, and the evaluation of losses and Q-factors.

A. RESONATOR DESIGN CONSIDERATIONS

The resonators are the basic elements of any coupled cavity filter. It is common practice to initiate the design procedure by optimizing the structure of the resonator to operate in the desired resonant mode and frequency range. The selection of the adequate resonator topology is indeed a fundamental step because it has a strong effect on the unloaded quality factor (Q_u), filter size, cost, and power handling capability of the complete filter.

Different cavity configurations for the resonators have been studied in [33], and the most suitable design has been chosen (see Fig. 1). Once the basic shape of the resonator has been defined, metallic screws are normally placed in the vicinity of the open-ended post to create a variable capacitance to tune the resonance at the desired frequency.

There are, however, several issues associated with the use of metallic tuning screws. Namely, the metallic screws must be securely fastened to the body of the filter. As a consequence, remote tuning becomes problematic. Additionally, even if a remote tuning mechanism could be developed, the structure would be extremely sensitive to the position of the metallic tuning screw, so that a practical (low-cost) solution for an actuator-controlled remote tuning would be very difficult to implement. Finally, metallic tuning screws can also introduce significant losses in the filter structure if repeated tuning is required. In our basic resonator, we have therefore replaced the traditional metal screws with dielectric tuners.

Additionally, as we can see in Fig. 1, a hollow metallic post has been chosen instead a solid one [32]. This has been done because a hollow post provides a support for the movement of the dielectric tuning element. Another reason for choosing this configuration is the almost-linear variation of the frequency with the tuner penetration. Using this configuration, we can, in fact, obtain the desired starting value of the resonant frequency using the metallic post, and we can then have an extended tuning range inserting a dielectric rod inside the cavity using the hollow post as a support.

The dimensional parameters of the basic resonator in Fig. 1 are: $l_0 = H = 50\,\text{mm}$ and $W = 40\,\text{mm}$. The outer and inner diameters of the hollow post are $D_o = 16\,\text{mm}$ and $D_i = 12\,\text{mm}$, respectively. The height of the hollow post is $h_0 = 32.290\,\text{mm}$. h_d is the height of the dielectric tuner, the diameter of which is $D = 11.8\,\text{mm}$ (slightly less than D_i).

Fig. 2 shows the variation in center frequency with the tuner penetration. The linear pattern is clearly evident. Fig. 2 shows also the unloaded quality factor Q_u as a function of the dielectric post penetration. The values for the Q_u are quite high ranging from 4200 for deep penetrations up to near 5600 for penetrations not exceeding the hollow post h_0. It is interesting to note that the equivalent structure with a metallic tuner has a quality factor of 2758 at the lowest frequency compared with the Q value of 4200 using the dielectric tuner. Furthermore, we have verified that, with the resonator we have designed, we can indeed tune the resonance in the entire frequency range of interest.

B. DESIGN CONSIDERATIONS OF INPUT AND OUTPUT COUPLING

In the context of tunable filters, it is very crucial to maintain the correct input/output coupling throughout the frequency tuning range in order to maintain constant bandwidth and

return loss levels. The Q_{ext} value is computed from the desired filter center frequency (f_0) and bandwidth (BW) using the following classical expression [6]:

$$Q_{\text{ext}} = \frac{f_0}{M_{S1}^2 BW} \tag{1}$$

where M_{S1} is the coupling matrix element corresponding to the input coupling of the filter.

From equation (1), we can now deduce the following:

1) For lower f_0 and constant BW a higher input coupling is required. Therefore, lower frequencies are more challenging for tunable filters.
2) For wider BW a lower Q_{ext} (higher input coupling) is also required. Therefore wider BW are more challenging for tunable filters.

As initially discussed in [33], we propose to use the structure shown in Fig. 3, where the resonator post and the input coupling post are attached to opposite walls. This geometrical configuration allows for a stronger electric coupling, thus providing the required coupling strength. The input coupling post shares the same mechanism as the tunable resonator: a dielectric rod is inserted inside the hollow post. This arrangement does indeed provide a variable capacitive coupling that depends on the penetration of the dielectric rod.

The dimensions of the structure in Fig. 3 have been chosen to be consistent with the dimensions of the basic resonator, namely, $l_0 = H = 50\,\text{mm}$ and $W = 40\,\text{mm}$, where the height of the hollow resonator and the coupling structure are $h_0 = 26.172\,\text{mm}$ and $h_i = 26.82\,\text{mm}$, respectively. The input coaxial feed is located at $h_c = 19.140\,\text{mm}$. The value of h_i is optimized to obtain the input coupling value that is required at the highest frequency, when the dielectric rod is fully inserted in the metallic post (Fig. 3). The inner conductor of the coaxial input is connected to the first metallic post at a height $h_c = 19.140\,\text{mm}$ which is 7.68 mm shorter than h_i. This has been done in order to ensure the proper mechanical robustness of the input structure. The outer diameter of the input/output metallic post is set at $d_0 = 8\,\text{mm}$. The inner diameter is $d_i = 6\,\text{mm}$ and the rod inserted inside has a diameter of 5.95 mm. A gap s equal to 2.0 mm has been left between the input post and the resonator post. The lowest coupling value is obtained when the dielectric rod is totally confined inside the metallic hollow post having height $h_{\text{id1}} = 25\,\text{mm}$.

A key point to be emphasized at this stage is that the input coupling in our combline cavity loads significantly the first resonator. This leads to a reduction in the height of the resonator post (please note that $h_0 = 26.172\,\text{mm}$ in Fig. 3, whereas $h_0 = 32.290\,\text{mm}$ in Fig. 1). This, in turn, allows for an enhanced range in the frequency tuning of the input resonator.

Fig. 4 shows the experiment carried out using the structure in Fig. 3. From this result, we can now see that, using (1), the Q_{ext} value required to maintain the $RL = 25\,\text{dB}$ at 1.842 GHz is around 18.5 while at 1.542 GHz (for $BW = 75\,\text{MHz}$), the Q_{ext} value required is 15.5. Fig. 4 confirms that our structure can provide the required coupling values in the frequency range of interest. Moreover, the variation of Q_{ext} slightly degrades the quality factor of the cavity (from 4280 to 3922), as also shown in Fig. 4.

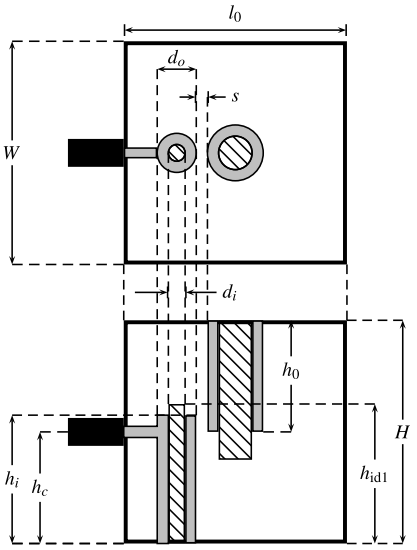

FIGURE 3. Input cavity configuration with the most significant geometrical parameters.

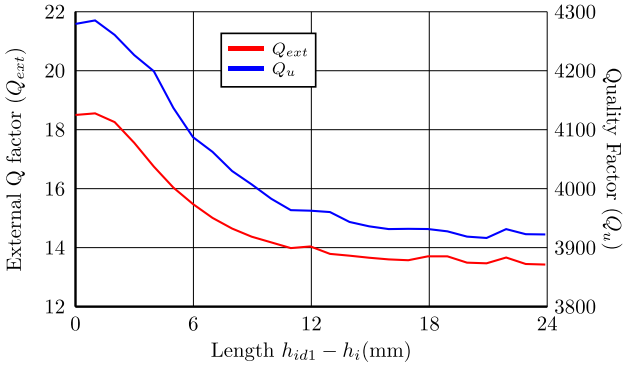

FIGURE 4. Q_{ext} (left side scale) and Q_u (right side scale) variation of the proposed solution. The x-axis shows the length of the dielectric rod exceeding the hollow post ($h_{\text{id1}} - h_i$).

An additional interesting point is that our simulations indicate that inserting the dielectric rod in the input coupling post lowers the resonant frequency of the cavity (it has been observed that it changes from 1.813 GHz for $h_{\text{id1}} - h_i = 0\,\text{mm}$ to 1.746 GHz for $h_{\text{id1}} - h_i = 24\,\text{mm}$). This is indeed a clear indication that confirms the capacitive nature of the input coupling.

C. DESIGN CONSIDERATIONS OF INTER-RESONATOR COUPLING

Generally speaking, a very common solution to implement the inter resonator coupling in combline filters is to use coupling windows (see for instance [34]). Metallic or dielectric tuning elements (or screws) are then located inside the coupling windows (2mm thick) to tune the coupling to the desired value (see the red inset in Fig. 5). However, our study

shows that using coupling windows and tuning elements is not adequate for the application under investigation. The reason is that the coupling value variations that can be achieved are insufficient for our application.

The solution that we propose in this paper consists of using a short hollow metallic post having an outer diameter of $d_0 = 8\,\text{mm}$, and an inner diameter of $d_i = 6\,\text{mm}$, with a dielectric tuner (of diameter 5.95 mm) inside, located on the wall opposite to the resonator post, in the middle between resonators (see the blue inset in Fig. 5). The rest of the dimensional variables (for the cavity resonator and dielectric tuner) are kept the same as the ones given in section II-A. The results in Fig. 5 show the coupling range obtained by full-wave simulation. The extraction of the coupling values has been carried out with two resonators weakly coupled to the input/output ports and strongly coupled to each other, as described in [6]. Another advantage of this solution is that the initial coupling value is then established with the height of the hollow metallic post $h_c = 11\,\text{mm}$. Another feature of this solution is that without a coupling window, the dielectric rod has more room to penetrate in the filter cavity, thus implementing a stronger coupling between resonators, as well as a wider range of coupling values. This is indeed confirmed by a comparison of the results shown in Fig. 5.

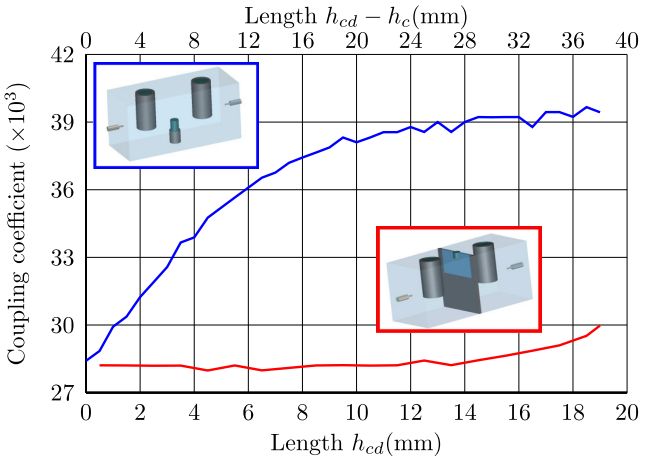

FIGURE 5. Inter-resonator coupling using a metallic post without a coupling window (upper side scale). The length of the hollow post holding the tuner is $h_c = 11$ mm. Length h_{cd} is the height of the dielectric tuner. Inter-resonator coupling using an iris with a dielectric tuning screw (lower side scale). h_{cd} is the height of the dielectric tuner. Blue line: response of coupling using a dielectric post. Red line: response of coupling using an iris.

D. COMPLETE FILTER GEOMETRY

The results that have been shown so far can effectively be used to establish the initial dimension of our filter structure.

The filter transfer function we want to implement is a fourth-order Chebyshev function. The desired specifications are as follows:

- Center frequency must be tunable from $f_{0,\min} = 1.542\,\text{GHz}$ up to $f_{0,\max} = 1.842\,\text{GHz}$.
- Bandwidth $BW = 75\,\text{MHz}$ constant throughout the whole range of frequencies.
- Return loss: $RL > 25\,\text{dB}$.

and must be achieved while maintaining a constant bandwidth and return loss performance. This means that the filter tuning range, as defined in [35], [36], and [37], for instance, is:

$$\frac{f_{0,\max} - f_{0,\min}}{f_C} \times 100 \approx 18\% \tag{2}$$

where f_C is given by:

$$\frac{f_{0,\max} + f_{0,\min}}{2} = 1.692\,GHz \tag{3}$$

and the relative bandwidth at f_C is $\approx 4.4\%$. Which means that the filter must be tuned over a frequency range that is approximately equal to four times the bandwidth (that is $\approx 400\%$ in terms of BW).

It is now interesting to note that, if we use the tunability range definition proposed in [5] and [22], we obtain directly:

$$\frac{f_{0,\max} - f_{0,\min}}{BW} \times 100 \approx 400\% \tag{4}$$

It is important to note that our definition of tunability does not intend to define the quality of a filter. The objective of the definition is simply to measure the tuning range in terms of the number of bandwidths. This second definition is, therefore, the one we will use in the reminder of this paper since we believe that it is more appropriate for tunable filters with constant bandwidth.

The procedure we have followed to actually design the filter is based on the group delay computation described in [6]. A lumped element model is used to obtain the reference values for the different stages. The dimensions of the real structure are obtained through optimization in a stage-by-stage procedure using CST Studio Suite (v.2022, Dassault Systémes) [38] in low precision (and without considering mechanization effects). The precision has been controlled by adjusting the computational variables, namely, the threshold of the convergence criteria, the number of passes/checks and the number of cells per max model box. Finally, with the space mapping technique described in [39], the final dimensions of the real structure are obtained using CST Studio Suite (v.2022, Dassault Systémes) for the high precision full-wave electromagnetic simulations.

Fig. 6 shows the 2D side view of the structure of the proposed filter. The final prototype consists of a single housing of dimensions $W \times H \times l$, with $W = 40\,\text{mm}$, $H = 50\,\text{mm}$ and $l = 200\,\text{mm}$, being W the width of the waveguide housing (transversal dimension not shown in Fig. 6). The resonators are located at $l_1 = 50\,\text{mm}$ and $l_2 = 50\,\text{mm}$. The height values of the hollow metal supports for the dielectric resonators and coupling structures are $h_1 = h_4 = 26.819\,\text{mm}$, $h_2 = h_3 = 30.651\,\text{mm}$, $h_i = 26.952\,\text{mm}$, $hc_1 = hc_3 = 19.681\,\text{mm}$, $hc_2 = 13.351\,\text{mm}$, respectively. All four hollow metal supports for the resonators have the same outer and inner diameter of $D_o = 16\,\text{mm}$ and $D_i = 12\,\text{mm}$, respectively. The outer diameter of all hollow metal

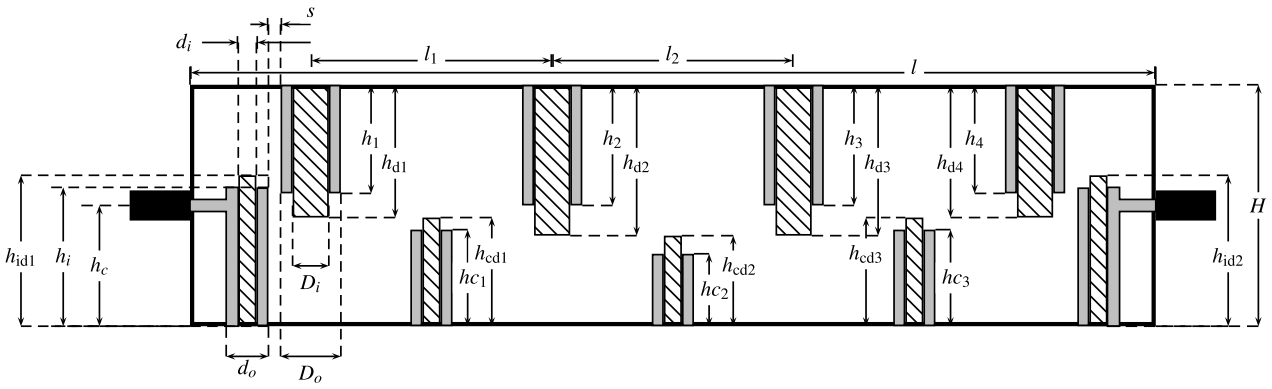

FIGURE 6. Side view of the filter structure. The filter is symmetric and the most relevant dimensions used in the design are shown.

supports for the coupling posts is $d_0 = 8$ mm, and the inner diameter is $d_i = 6$ mm. The gap s has been set to 2.0 mm to facilitate manufacturing. The coaxial connector (of external and internal diameters equal to 4.06 mm and 1.28 mm, respectively, with dielectric constant 2.1) is placed at a height of $h_c = 24.528$ mm for the input/output excitation.

It is important to point out at this stage that the starting values for the resonators, input and output couplings and inter-resonator couplings are simply obtained by optimizing the height of hollow metallic support cylinders, while keeping the dielectric rods inside the support structures. The Alumina dielectric rods, with a dielectric constant of 9.9 and loss tangent of 0.0002, are then pushed out of the hollow support posts in order to tune the filter at a lower center frequency. For this purpose, the diameters of the tuners used in the resonator and coupling structures are 11.8 mm and 5.95 mm, respectively. They are slightly smaller than the inner diameters of the corresponding hollow metal supports.

The two extreme cases for the tuning range have been obtained with the penetrations of the Alumina tuners shown in Table 1. The simulated filter performance for these two cases is shown in Fig. 7. The inset in Fig. 7 shows a detailed view of the insertion losses at the lower and upper end of the tuning range. The structure has been simulated considering the losses due to aluminum for all metal parts, and the losses for the dielectric tuning rods (Alumina). The simulations have been carried out with two different full-wave 3D simulators, namely, HFSS (Ansoft) and CST Studio Suite, in order to validate the accuracy of the results obtained. Moreover, the quality factor has been estimated using the simulation results including all losses.

As we can see, the proposed structure maintains the same filter characteristics for a tuning range of 300 MHz. The insertion loss is better than 0.06 dB when the filter is tuned at $f_{0,\min} = 1542$ MHz, giving an estimated quality factor approximately equal to 5982. When the response is tuned at $f_{0,\max} = 1842$ MHz, on the other hand, the insertion losses are better than 0.05 dB with a quality factor approximately equal to 7430.

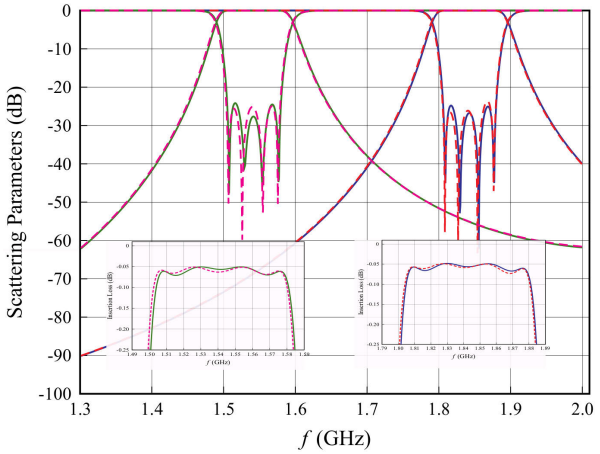

FIGURE 7. Electrical response of the filter for two extreme cases of the tuning range (the upper frequency case requires the lowest penetrations of the tuners and the lower frequency case requires the deepest penetrations). Solid lines: simulation with CST. Dashed lines: simulation with HFSS (Insertion loss response in corresponding inset figure).

III. ZIRCONIA VS ALUMINA TUNERS

In the previous section, we have shown how the structure that we propose can effectively be used to build combline filters that can be tuned in center frequency using tuning rods made of Alumina. In this section we explore the use of an alternative dielectric, namely, Zirconium Dioxide ($Y_2O_3 - ZrO_2$), or simply Zirconia. This material has, in fact, already been proposed for a number of microwave applications.

In [40], for instance, the performance of Zirconia thick films in high Q structures has been studied. Moreover, [41] has carried out comparative studies of Yttrium-stabilized Zirconia and Alumina coatings. Furthermore, the use of Zirconia in wideband filter applications has also been recently shown in [42]. The Zirconia we have use has the dielectric constant $\epsilon_r = 28$, and loss tangent $\tan\delta = 0.001$.

A. RESONATOR RESULTS

Having changed the dielectric material, we need also to redesign the basic resonator. The dimensions of the center

TABLE 1. Simulated dielectric tuners penetration (in mm).

Frequency (GHz)	h_{id1}	h_{d1}	h_{cd1}	h_{d2}	h_{cd2}	h_{d3}	h_{cd3}	h_{d4}	h_{id2}
1.842 GHz	25 mm	24 mm	16.5 mm	29 mm	12 mm	29 mm	16.5 mm	24 mm	25 mm
1.542 GHz	44.56 mm	45.07 mm	49.9 mm	47.75 mm	18 mm	47.75 mm	49.9 mm	45.07 mm	44.56 mm

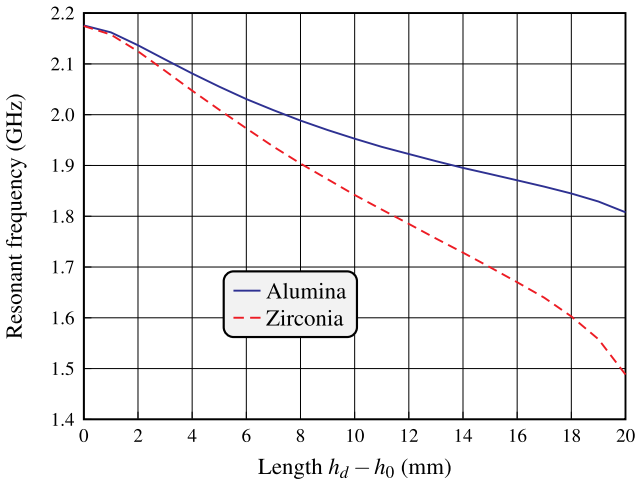

FIGURE 8. Resonant frequency in terms of the penetration of the dielectric rod exceeding the hollow post ($h_d - h_0$) according to Fig. 1.

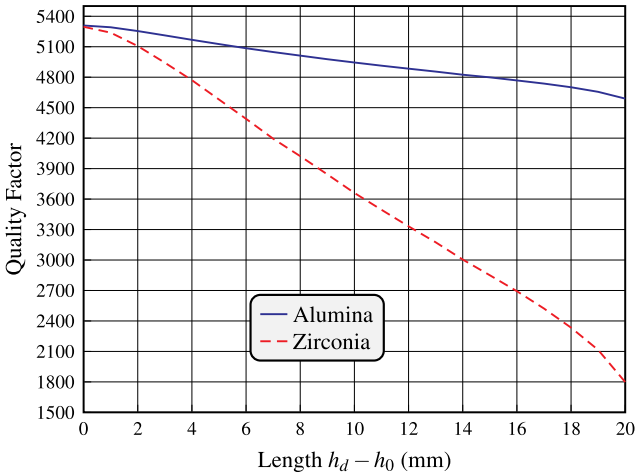

FIGURE 9. Q_u factor in terms of the penetration of the dielectric rod exceeding the hollow post ($h_d - h_0$) according to Fig. 1.

resonator post are calculated following the same procedure already discussed. The resulting cavity dimensions (shown in Fig. 1) are $l_0 = 44.8$ mm, $H = 48$ mm and $W = 35$ mm. The hollow resonator post is set to $h_0 = 27.5$ mm in order to place the initial resonant frequency (the highest one of the new design) at $f_0 = 2.175$ GHz.

One point that is now important is to make sure that the use of a higher dielectric constant does not introduce radiation loss. Radiation could, in fact, occur because the metallic posts loaded with Zirconia are actually sections of circular waveguide. If their cutoff is near the resonant frequency of the cavity, they could effectively extract energy from the filter. The diameter that we have used for the dielectric rod is $D = 9.91$ mm. The hollow post has an inner diameter $D_i = 10$ mm. The resulting cutoff frequency is 3.39 GHz, which is well above the maximum operating frequency of our filter. Another important consideration in this context is that all the hollow posts are located along the center line of the filter. As a consequence, due to symmetry, the excitation of the modes inside the hollow posts is theoretically reduced to zero. The above considerations confirm that the structure we have chosen does not suffer from losses due to radiation.

One advantage introduced by the use of Zirconia is that the tuning range is considerably extended with respect to Alumina, as shown in Fig. 8. However, a significant effect in the unloaded quality factor is observed, as shown in Fig. 9.

B. RESULTS FOR INTER RESONATOR COUPLING

In this new design, we have used a different approach to fix the initial inter-resonator coupling. The correct coupling value has, in fact, been obtained optimizing the distance between the consecutive resonator posts (l_1 and l_2 variables in Fig. 6), rather than the height of the hollow inter-resonator post. However, a hollow metallic post of $= 5$ mm in height has been maintained to provide mechanical support for the dielectric rods. An additional advantage of using Zirconia is that it provides a much stronger (and relatively linear) variation of the coupling coefficient, as compared to the one in Fig. 5. To simplify the manufacturing, the outer and inner diameters of the metallic posts are chosen to be $D_0 = 12$ mm and $D_i = 10$ mm (the same as in the resonators). A distance between two resonator posts of $l_1 = 44$ mm is, in this case, required to obtain the initial coupling coefficient value equal to 0.0185.

Furthermore, a dielectric rod of the diameter $D = 9.91$ mm is inserted inside the hollow post. It is important to note that, for the sake of comparison, we have used for this study the two types of dielectric rods (Zirconia and Alumina) with the same dimensions. The results of this experiment clearly show significantly wider coupling range values with Zirconia, as shown in Fig. 10.

C. RESULTS FOR INPUT/OUTPUT COUPLING

We re-designed next the input coupling structure in Fig. 3. The resulting dimensions are $H = 48$ mm, $l_0 = 44$ mm and $W = 35$ mm. The height of the hollow resonator post and the input coupling structure are $h_0 = 24.2$ mm and $h_i = 22.35$ mm, respectively. The coaxial input probe has been placed at the height $h_c = 21$ mm. The hollow post now

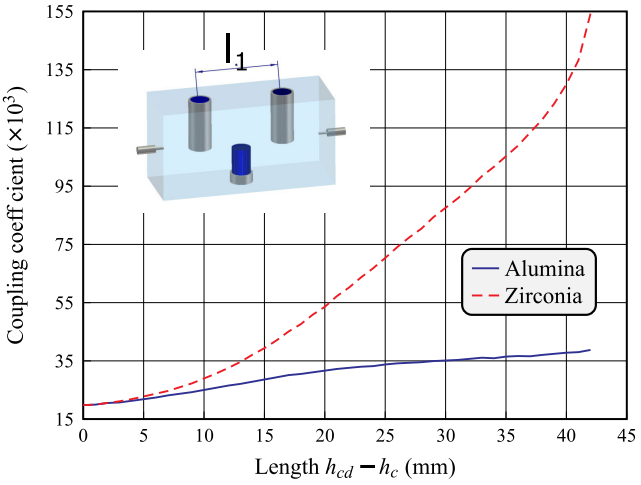

FIGURE 10. Coupling coefficient variation for two possible cases: experiment with Alumina (solid line) and the proposed solution using Zirconia (dashed line). Distance l_1 in the inset has been moved to obtain the initial coupling value at the left of the graph. Both coupling coefficients are plotted versus the penetration of the dielectric tuner exceeding the hollow post ($h_{cd} - h_c$).

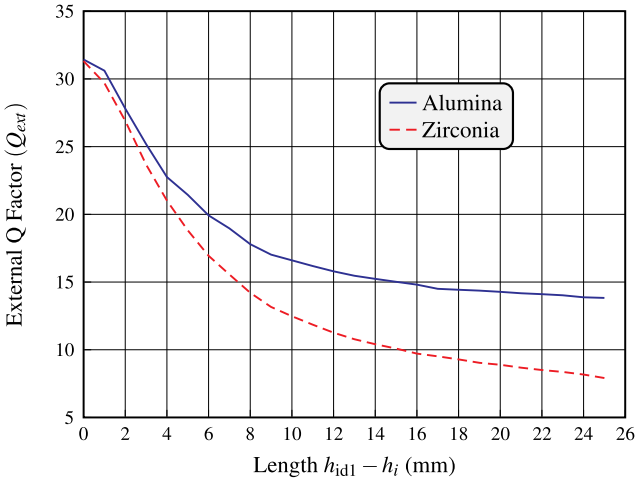

FIGURE 11. Q_{ext} variation for two possible cases: experiment with Alumina (solid line) and the proposed solution inserting Zirconia (dashed line). Both curves are plotted versus the penetration of the dielectric rod exceeding the hollow post ($h_{id1} - h_i$).

has outer and inner diameters equal to $d_o = 12$ mm and $d_i = 10$ mm, respectively. The dielectric rods of Alumina and Zirconia are inserted to explore the variation in the input coupling value. A gap s equal to 2 mm has been left between the coupling post and the resonator post.

In order to start the experiment, the dielectric rod is totally confined inside the metallic hollow post having height equal to $h_{id1} = 22$ mm. The simulations we have performed indicates that the structure provides a $Q_{ext} = 32.8$. This is indeed the value required to design the initial case (highest center frequency of 2.175 GHz and lower bandwidth of 50 MHz). As expected, Zirconia can achieve a significantly wider range of Q_{ext} with respect to the h_{id1}, as shown in Fig. 11.

IV. TUNABLE FILTER IN FREQUENCY AND BANDWIDTH

Using the information obtained with respect to the behavior of Zirconia, we have next re-designed the filter structure using the same procedure already described for the Alumina case in Fig. 6. The novel prototype consists of a single housing (see Fig. 6) of dimensions $W \times H \times l$ with $W = 35$ mm, $H = 48$ mm and $l = 177.8$ mm.

As previously discussed in section III-B, in this case we have optimized the length between consecutive resonators to obtain the initial values for the inter resonator couplings. This leads to the initial values $l_1 = 41.82$ mm and $l_2 = 46.12$ mm. The height of the hollow resonator posts are set to $h_1 = h_4 = 24.45$ mm and $h_2 = h_3 = 26.82$ mm. All inter-resonator coupling hollow posts have equal height of $hc_1 = hc_2 = hc_3 = 5$ mm that also act as the support structures for the dielectric tuners. In order to simplify the structure, all the hollow metallic posts used for either inter resonator couplings and input/output couplings are set to the same outer diameter of $d_o = D_o = 12$ mm. All inner diameters are set to $d_i = D_i = 10$ mm, which allows the same size dielectric rod ($D = 9.91$ mm) to be utilized for all the tuning elements.

The input coupling post having the height of $h_i = 22.37$ mm has been excited with a coaxial probe at the height of $h_c = 21$ mm. The gap s has been set to 2mm to simplify manufacturing. The coaxial connector for the input and output excitation is the same used in section II.

In order to provide an accurate prediction of the filter performance, the structure has been simulated taking into account the metal losses in the aluminum for the hollow posts and the housing. Dielectric losses are also taken into account in all rods used for the resonators and for the coupling structures. It is important to note that the filter structures discussed in this paper are reconfigurable also in bandwidth in addition to center frequency. For this last filter, for instance, the lower and upper limits of the bandwidth are $BW = 50$ MHz and $BW = 100$ MHz, respectively. This means that the filter can be tuned to achieve any bandwidth value between 50 MHz to 100 MHz throughout the complete center frequency tuning range while maintain an equiripple return loss $RL > 25$ dB in all cases. The specifications for the initial design of this fully reconfigurable filter are as follows:

Case 1:

- Center frequency must be tunable from $f_{0,\min} = 1.475$ GHz up to $f_{0,\max} = 2.175$ GHz.
- Bandwidth $BW = 50$ MHz constant throughout the whole range of frequencies.
- Return losses: $RL > 25$ dB.

and must be achieved while maintaining a constant 50MHz bandwidth and return loss performance. This means that the filter tuning range (as defined in [5] and [22]) is

$$\frac{f_{0,\max} - f_{0,\min}}{BW} \times 100 = 1400\% \tag{5}$$

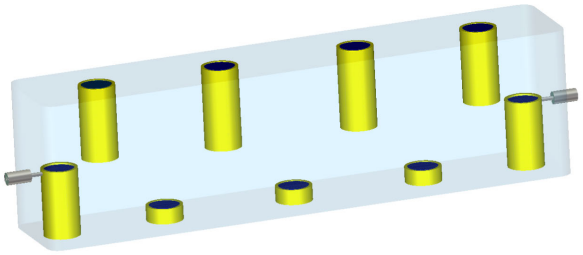

FIGURE 12. 3-D model of the combline filter with tunable frequency and bandwidth.

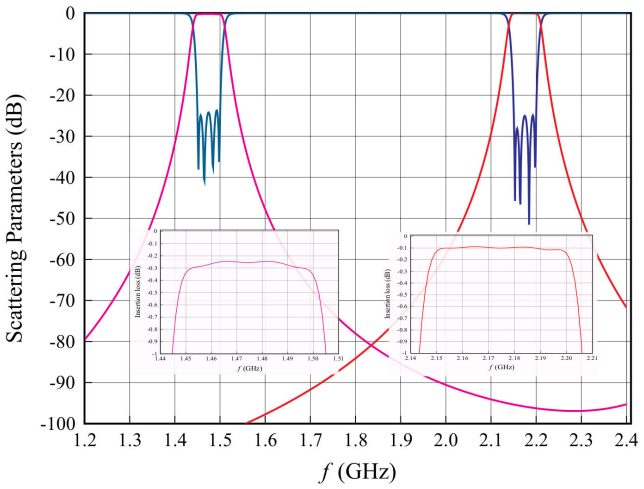

FIGURE 13. Simulation response of the filter for two extreme cases of the tuning range (the upper frequency case requires the lowest penetrations of the tuners, and the lower frequency case requires the deeper penetrations) while keeping the initial 50 MHz bandwidth. Blue line: Simulated S_{11} at 2175 MHz. Red line: Simulated S_{21} at 2175 MHz. Midnight Blue line: Simulated S_{11} at 1475 MHz. Magenta line: Simulated S_{21} at 1475 MHz (Insertion loss in corresponding inset figure).

Case 2:

- Center frequency must be tunable from $f_{0,\min} = 1.60\,\text{GHz}$ up to $f_{0,\max} = 1.92\,\text{GHz}$.
- Bandwidth $BW = 100\,\text{MHz}$ constant throughout the whole range of frequencies.
- Return losses: $RL > 25\,\text{dB}$.

This means that the filter tuning range (as defined in [5] and [22]) is

$$\frac{f_{0,\max} - f_{0,\min}}{BW} \times 100 = 320\% \tag{6}$$

Fig. 12 shows the final structure of the filter. As we can see, for case 2 ($BW = 100\,\text{MHz}$) the frequency tuning range is smaller than for case 1 ($BW = 50\,\text{MHz}$). This is due to the loading effect of the dielectric tuners, which need to be pushed out of the hollow posts in the coupling elements to obtain a wider bandwidth ($BW = 100\,\text{MHz}$), thus reducing the maximum frequency value that can be achieved. The penetration of the Zirconia tuners is summarized in Table 2 for the lower and higher cases of the lowest (50 MHz) and highest (100 MHz) filter bandwidths.

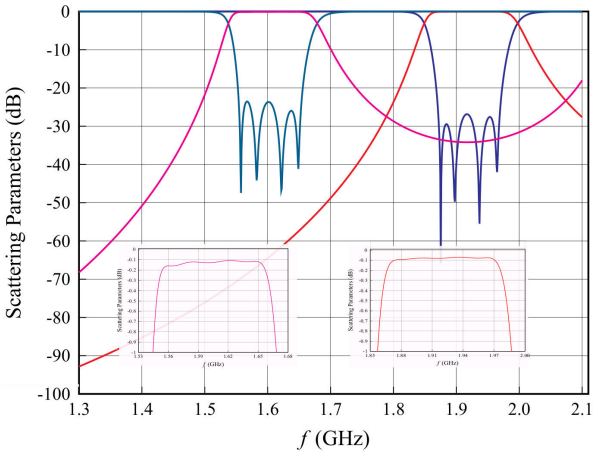

FIGURE 14. Simulation response of the filter for two extreme cases of the tuning range (the upper frequency case requires the lowest penetrations of the tuners, and the lower frequency case requires the deeper penetrations) while keeping the 100 MHz bandwidth. Blue line: Simulated S_{11} at 1920 MHz. Red line: Simulated S_{21} at 1920 MHz. Midnight Blue line: Simulated S_{11} at 1600 MHz. Magenta line: Simulated S_{21} at 1600 MHz (Insertion loss response in corresponding inset figure).

Fig. 13 shows the simulated performance obtained by changing the filter center frequency while maintaining a constant bandwidth of 50 MHz. Fig. 14, on the other hand, shows the simulated performance obtained maintaining a constant bandwidth of 100 MHz. It is worth noting at this stage that our simulations predicted the in-band insertion loss of 0.3 dB for 50 MHz and 0.25 dB for 100 MHz. These theoretical values are in good agreement with the experimental results of the manufactured prototype shown next.

V. EXPERIMENTAL RESULTS AND DISCUSSION

The manufacturing drawings of the filter prototype have been obtained using SolidWorks (from Dassault Systémes SolidWorks Corp.). The structure is composed of one body and two covers. Fig. 15 shows the 3D model of the filter.

As shown in Fig. 15, an additional 10 mm length of hollow metallic post is added to the external surface of both top and bottom covers. This has been done to provide mechanical support to the dielectric rods. Furthermore, a Teflon screw has been added in the orthogonal direction, to hold the dielectric rods in the desired tuning position. It is important to note at this point that, due to the use of milling, all concave corners of the filter body now have a curvature radius equal to 2 mm. The filter is made in Aluminum without silver plating.

Fig. 16 shows the internal topology of the filter before assembly. Furthermore, Fig. 17 shows the prototype of the filter assembles using dielectric tuners made of Zirconia. The filter has been tested using a vector network analyzer (VNA), after being properly calibrated following a standard TRL procedure. The filter is initially tuned at the higher center frequency of 2175 MHz with the lowest $BW = 50\,\text{MHz}$. Then, as it has already been discussed, the bandwidth of the

TABLE 2. Simulated Zirconia tuners penetration (in mm).

Frequency (GHz)	Bandwidth (MHz)	h_{id1}(mm)	h_{d1}(mm)	h_{cd1}(mm)	h_{d2}(mm)	h_{cd2}(mm)	h_{d3}(mm)	h_{cd3}(mm)	h_{d4}(mm)	h_{id2}(mm)
2.175 GHz	50 MHz	22	24	5	26.4	5	26.4	5	24	22
1.475 GHz	50 MHz	30.10	44.60	15.77	46.8	13.93	46.8	15.77	44.60	30.10
1.920 GHz	100 MHz	32.28	23.86	30.63	30.94	27.65	30.94	30.63	23.86	32.28
1.600 GHz	100 MHz	41.68	31.28	46.99	41.06	44.62	41.06	46.99	31.28	41.68

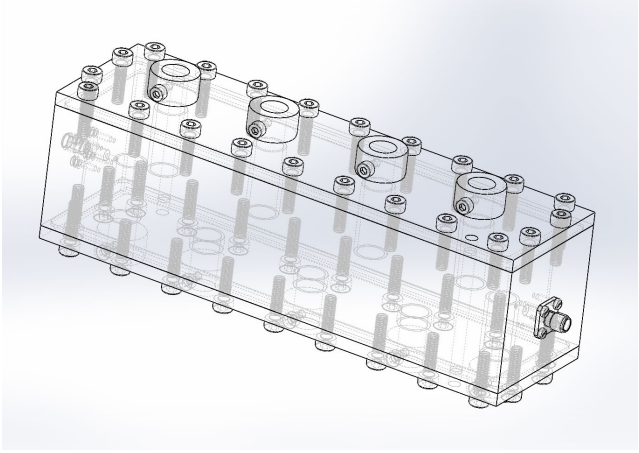

FIGURE 15. Final structural model (developed with SolidWorks) of the filter prototype.

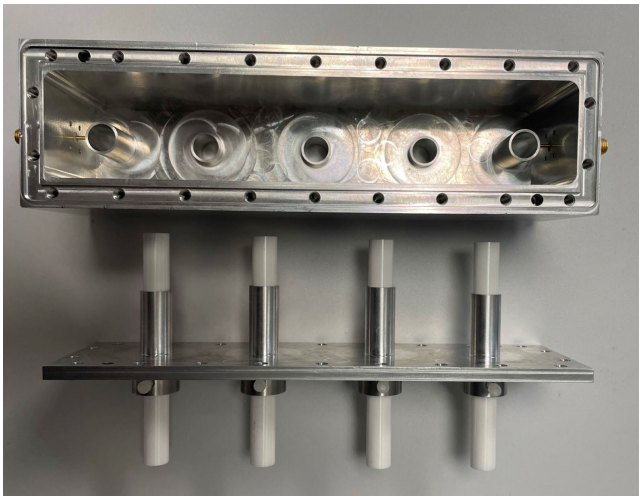

FIGURE 16. Filter structure before assembly.

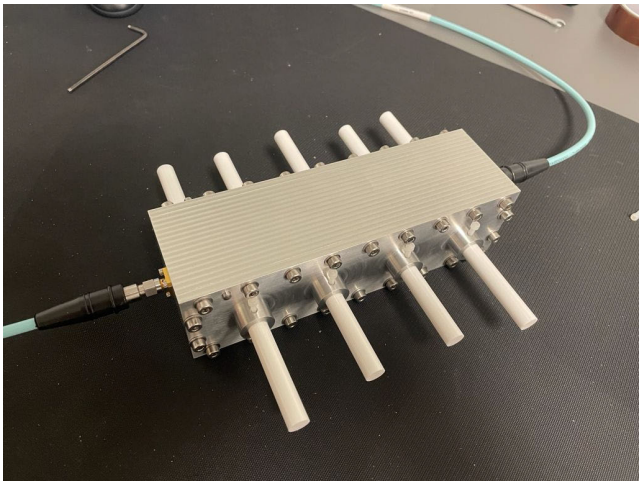

FIGURE 17. Final assembled filter prototype on the test bench.

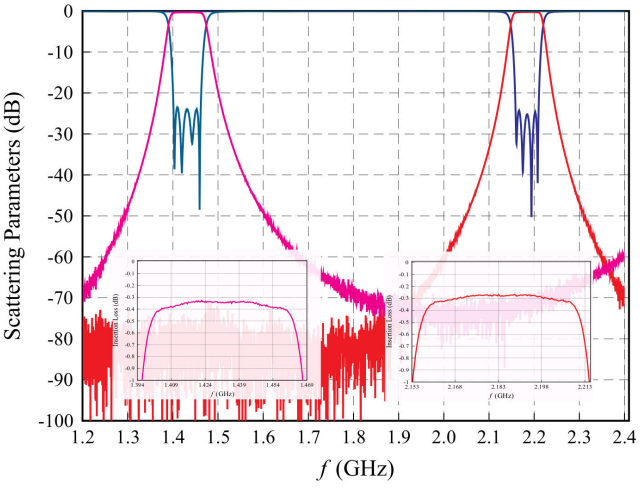

FIGURE 18. Measured response of the filter for two extreme cases of the tuning range while keeping the initial 50 MHz bandwidth. Blue line: Measured S_{11} at 2180 MHz. Red line: Measured S_{21} at 2180 MHz. Midnight Blue line: Measured S_{11} at 1433 MHz. Magenta line: Measured S_{21} at 1433 MHz (Insertion loss response in corresponding inset figure).

bandpass response can be tuned to any value between 50 MHz and 100 MHz, in the corresponding frequency ranges. As a proof of concept, the two extreme cases (i.e. $BW = 50$ MHz and $BW = 100$ MHz) have been demonstrated. In the first case, the filter center frequency can be tuned while keeping a constant bandwidth equal to 50 MHz, as shown in Fig. 18. The achieved frequency tuning range is 1494%, namely, from 1433 MHz to 2180 MHz. The response of the filter has an insertion loss level better than 0.35 dB throughout the complete tuning range, as shown in the inset of Fig. 18.

The next measurement has been performed expanding the bandwidth up to 100 MHz (double of the initial bandwidth). In this case, the filter can achieve a tuning range of 320%, starting from 1600 MHz down to 1920 MHz. As shown in Fig. 19, the measured results show a return loss level always better than 25 dB, and insertion loss values below 0.22 dB through the whole tuning range.

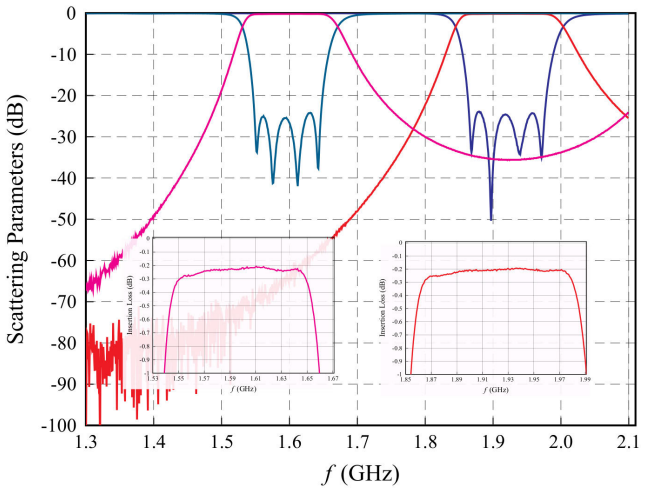

FIGURE 19. Measured response of the filter for two extreme cases of the tuning range while keeping the initial 100 MHz bandwidth. Blue line: Measured S_{11} at 1920 MHz. Red line: Measured S_{21} at 1920 MHz. Midnight Blue line: Measured S_{11} at 1600 MHz. Magenta line: Measured S_{21} at 1600 MHz (Insertion loss response in corresponding inset figure).

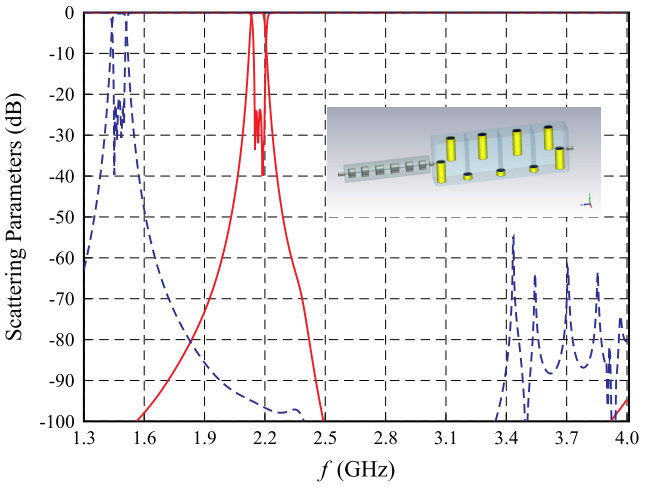

FIGURE 20. Simulated response of the integrated structure with LPF for two extreme cases of the tuning range while keeping the initial 50 MHz bandwidth. Red line: Simulated response at 2175 MHz. Blue dashed line: Simulated response at 1475 MHz. (Lowpass filter + Bandpass filter integrated structure in corresponding inset figure).

One important aspect to evaluate the performance of our filter structure is the achieved quality factor. To this end, the Q factor has been evaluated and compared using the insertion loss of the measured and simulated responses [43]. The results obtained are shown in Table. 3. The frequency range used is $1475 - 2175$ MHz. The extracted Q factor from measurement appears to be in agreement with the simulated estimations. It is important to note at this point that the prototype has been manufactured using aluminum. The Q factor of the filter can be further improved using silver plating, as can be seen in [44].

VI. OUT-OF-BAND PERFORMANCE

One of the key characteristics of any microwave filter is the out-of-band performance. However, the specific requirements that a filter must satisfy are normally dictated by the intended application. In this context, therefore, since the main objective of this paper is to discuss the proof-of-concept for a filter structure that can be reconfigured both in terms of center frequency and bandwidth, we are not aiming at satisfying a specific set of requirements. Nevertheless, since the out-of-band performance is indeed an important aspect, we discuss in this section a number of examples of how the spurious performance of our filter can be easily controlled with the help of simple, standard lowpass filters (LPFs).

Generally speaking, the out of band performance of a filter is limited by the appearance of spurious responses that can be due to the harmonics of the resonators, or to the excitation of higher order modes. For the reconfigurable filter discussed in this paper, the out-of-band response is intrinsically linked to the filter bandwidth. In fact, increasing the bandwidth, will inevitably reduce the spurious free range above the filter passband.

As a first illustrative example, we have designed a simple six-pole stepped-impedance coaxial lowpass filter, with a cutoff frequency of 2.3 GHz [45]. Fig. 20 shows the structure of the LPF integrated with the reconfigurable filter, and the simulated response for the case in which the bandwidth is set to the minimum value of 50 MHz. As we can see, adding a simple LPF of sixth order, we have obtained more than 60 dB of rejection up to 4 GHz.

As a second example, we have set the bandpass of our reconfigurable filter to 100 MHz, and we have designed an eight-pole coaxial LPF with a cutoff frequency of 2.02 GHz. Fig. 21 shows the structure and the simulated response. As expected, the LPF does improve the out-of-band response.

As a final example, we have demonstrated the combined case of an integrated lowpass filter with all the frequency and bandwidth scenarios. In this example, we have varied the bandwidths from 50 to 100 MHz. In this case, we have used an eight-pole LPF with a cutoff frequency set at 2.23 GHz. As we can see from Fig. 22, also in this case, a simple LPF can be used to improve the out-of-band response. In this case, however, the minimum frequency to which the filter can be tuned is limited to 1750 MHz, instead of 1600 MHz for 100 MHz bandwidth, as shown in Fig. 22.

The dimensions of the LPFs used in these three illustrations are given in Table 4. In all the lowpass filters discussed, the internal air spaces are filled with Teflon (relative permittivity value of 2.2). The input and output connector dimensions are identical to the ones of the filter described in subsection II-D.

VII. MULTIPACTION ANALYSIS

The power handling capability of microwave filters is a key issue for many applications and, as it is well-known, it must be evaluated in detail for each specific new structure that

TABLE 3. Q-values extracted from measurements and simulations.

Bandwidth (MHz)	Q-values extracted from measurements			Q-values extracted from simulations		
——	Frequency	Insertion loss at f_0(dB)	Q factor	Frequency	Insertion loss at f_0(dB)	Q factor
50 MHz	2180 MHz	0.320	2476	2175 MHz	0.102	7450
50 MHz	1433 MHz	0.341	1526	1475 MHz	0.255	2021
100 MHz	1920 MHz	0.202	1776	1920 MHz	0.079	4245
100 MHz	1600 MHz	0.215	1387	1600 MHz	0.129	2167

TABLE 4. Lowpass filter dimentions (in mm).

Cutoff Freq. (GHz)	l_{01}	l_{02}	l_{03}	l_{04}	l_{05}	l_{06}	l_{07}	l_{08}	l_{09}	R_{01}	R_{02}	R_{03}	R_{04}	R_{05}	R_{06}	R_{07}	R_{08}	R_{09}
2.3	0.647	7.792	9.186	8.224	10.34	9.973	9.755	——	——	1.968	5.062	0.593	5.568	0.619	5.358	0.552	——	——
2.02	0.519	5.989	10.81	8.227	10.18	9.614	8.718	10.82	8.863	1.392	5.832	0.646	6.143	0.443	6.016	0.290	5.876	0.311
2.23	0.535	5.022	9.169	7.203	9.359	8.067	7.324	9.427	7.759	0.942	5.784	0.519	5.991	0.422	5.936	0.222	5.767	0.273

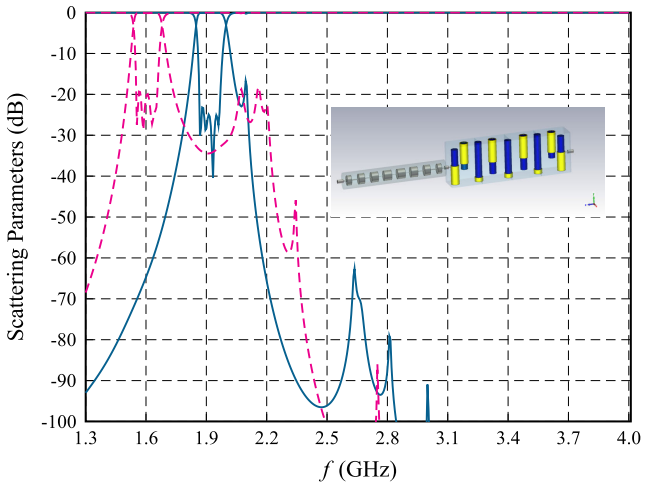

FIGURE 21. Simulated response of the integrated structure with LPF for two extreme cases of the tuning range while keeping the initial 100 MHz bandwidth. Midnight Blue line: Simulated response at 1920 MHz. Magenta dashed line: Simulated response at 1600 MHz. (Lowpass filter + Bandpass filter integrated structure in corresponding inset figure).

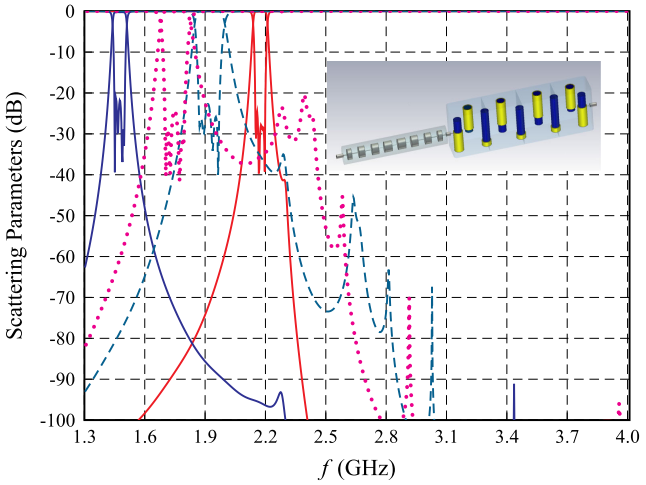

FIGURE 22. Simulated response of the integrated structure with LPF for extreme cases of the tuning range. Red line: Simulated response at 2175 MHz. Blue line: Simulated response at 1475 MHz. Midnight Blue dashed line: Simulated response at 1920 MHz. Magenta dotted line: Simulated response at 1750 MHz. (Lowpass filter + Bandpass filter integrated structure in corresponding inset figure).

is being developed. We, therefore, discuss in this section the results of a multipactor breakdown analysis for our reconfigurable filter [46]. It is important to note, however, that multipaction discharge can only happen in vacuum. As a consequence, we do not anticipate any power restrictions for ground applications.

To continue, it is important to note that, early in the design process of any filter, it is critical to evaluate and assess the power-handling phenomena of the structure being designed. In this context, the following are some key considerations relevant to multipaction:

- Coupling windows are very often critical for multipactor breakdown. As a consequence, structures without coupling windows can improve the power performance.
- The critical areas of the filter structure, namely, where the maximum electric field is located, must be identified so that a minimum gap can be used to avoid breakdown [47].
- Furthermore, since our filter structure uses both aluminum and dielectrics, the secondary emission yield (SEY) profile of the dielectric material is assumed to be the same as that of aluminum [48].
- The multipaction analysis requires the precise evaluation of the electromagnetic fields in the critical areas. The critical areas must therefore be identified, and a dense local meshing must be used to ensure the accuracy of the simulations using CST Studio Suite.

To continue, the parameters we used for the multipactor analysis, as required by the ECSS-E-HB-20-01A– Multipactor handbook [49], are as follows:

A. ALUMINUM

- SEY_{max}: 2.92.
- SEY_0: 0.8.
- E_1(eV), Impact energy: 17 eV.
- E_{max}(eV), Impact energy @ SEY_{max}: 276 eV.

TABLE 5. Simulated multipaction threshold comparison (in Watt).

Frequency Case (MHz)	Bandwidth (MHz)	Peak Power (W) @f_{min}		Peak Power (W) @f_0		Peak Power (W) @f_{max}	
2175	50	3843.62	@2.15 GHz	3656.12	@2.175 GHz	4031.12	@2.2 GHz
1720	50	137.69	@1.695 GHz	240.23	@1.72 GHz	496.08	@1.745 GHz
1670	50	90.82	@1.645 GHz	147.46	@1.67 GHz	110.35	@1.695 GHz
1620	50	46.38	@1.595 GHz	76.66	@1.62 GHz	55.17	@1.645 GHz
1571	50	19.67	@1.546 GHz	31.00	@1.571 GHz	24.17	@1.596 GHz
1545	50	16.23	@1.52 GHz	19.41	@1.545 GHz	17.21	@1.57 GHz
1475	50	4.55	@1.45 GHz	5.92	@1.475 GHz	7.87	@1.5 GHz
Frequency Case (MHz)	Bandwidth (MHz)	Peak Power (W) @f_{min}		Peak Power (W) @f_0		Peak Power (W) @f_{max}	
1920	100	1984.31	@1.87 GHz	1734.3	@1.92 GHz	1984.31	@1.97 GHz
1645	100	145.5	@1.595 GHz	205.07	@1.645 GHz	244.13	@1.695 GHz
1600	100	40.77	@1.55 GHz	120.11	@1.6 GHz	165.04	@1.65 GHz

B. POWER LOOP

- Precision: 0.1 dB.
- Initial Power: 500 W.
- Maximum Power: $1e + 06$ W.
- The initial number of electrons: 2000.

The power threshold has been estimated using SPARK3D v2022 (Aurora Software and Testing S.L.U., CST/3DS). The frequencies at which the multipaction threshold have been evaluated are three, namely, the center frequency and the ones at the edges of the bandwidth. The maximum peak power that we obtained for different cases in the tuning range is shown in Table 5. As we can see in Table 5, the filter structure is able to support a continuous wave of around 3656.12 W at the highest center frequency, as shown in row 1 of Table 5 for a 50 MHz bandwidth. However, as expected, there is significant degradation of power handling in the lower tuning frequency of 1475 MHz. When the filter is tuned to a bandwidth of 100 MHz, a similar pattern can be observed, as shown in the second section of Table 5.

It is therefore evident that there is a relation between the maximum power and the minimum tuning frequency. As an illustrative example, for instance, if we assume that the maximum required power is 100 W CW, the filter can be tuned from 2175 MHz to 1720 MHz (for 50 MHz bandwidth) and from 1920 MHz to 1645 MHz (for 100 MHz bandwidth).

Finally, it is important to note that, if higher power and a wider tuning range are required, enclosure of the filter structure in a pressurized environment would allow to use the full tuning range that the structure can offer.

VIII. REMOTE FILTER OPERATION

One important feature of the family of filters described in this paper, is that the use of dielectric tuners opens the possibility of developing remotely operated reconfigurable filters based on the use of low-cost, computer-controlled linear actuators.

In particular, this feature can be appreciated noting that, using the data in Table 2 for the central dielectric coupling rod movements, we obtain 13 μm/MHz for the 50 MHz bandwidth, and 57 μm/MHz for the 100 MHz bandwidth case.

These values are indeed perfectly compatible with commercial computer-controlled, low-cost linear actuators. Furthermore, it is important to note that, even though each tuner needs to be operated independently, developing the appropriate software, the complete filter performance can be controlled with a single command.

IX. CONCLUSION

In this paper, we have explored novel configurations to develop fully reconfigurable combline filters. The solution that we propose is based on the use of dielectric tuners. All resonators and all couplings can be tuned independently. The main advantage of using dielectrics is that it greatly reduces the sensitivity of the filter performance with respect to the position of the tuners. As a result, the use of a low-cost computer-controlled linear actuator becomes now an attractive possibility for the implementation of remotely reconfigurable combline filters. The out-of-band performance of our filter is also discussed, showing how a simple low-pass filter can be used to satisfy specific requirements. Furthermore, the multipaction power threshold of the structure has been studied, clearly showing that there is a trade-off between the maximum power and the minimum tuning frequency in vacuum. In conclusion, with the results presented in this paper, we have firmly established the proof of concept of a novel family of combline filters that is reconfigurable over a wide range of both bandwidth and center frequency. It is our opinion that the structure that we propose, may prove to be a significant contribution to the development of future reconfigurable payloads for both ground and space applications.

REFERENCES

[1] A. L. Allison, *The ITU and Managing Satellite Orbital and Spectrum Resources in the 21st Century* (SpringerBriefs in Space Development). Cham, Switzerland: Springer, 2014.

[2] G. Varrall, *Making TelecomsWork: From Technical Innovation to Commercial Success*. Chichester, U.K.: Wiley, 2012.

[3] J.-S. Hong, "Reconfigurable planar filters," *IEEE Microw. Mag.*, vol. 10, no. 6, pp. 73–83, Oct. 2009.

[4] R. R. Mansour, F. Huang, S. Fouladi, W. D. Yan, and M. Nasr, "High-*Q* tunable filters: Challenges and potential," *IEEE Microw. Mag.*, vol. 15, no. 5, pp. 70–82, Jul. 2014.

[5] E. Laplanche, N. Delhote, A. Périgaud, O. Tantot, S. Verdeyme, S. Bila, D. Pacaud, and L. Carpentier, "Tunable filtering devices in satellite payloads: A review of recent advanced fabrication technologies and designs of tunable cavity filters and multiplexers using mechanical actuation," *IEEE Microw. Mag.*, vol. 21, no. 3, pp. 69–83, Mar. 2020.

[6] R. J. Cameron, C. M. Kudsia, and R. R. Mansour, *Microwave Filters for Communication Systems: Fundamentals, Design, and Applications*, 2nd ed. Hoboken, NJ, USA: Wiley, 2018.

[7] M. Yu, B. Yassini, B. Keats, and Y. Wang, "The sound the air makes: High-performance tunable filters based on air-cavity resonators," *IEEE Microw. Mag.*, vol. 15, no. 5, pp. 83–93, Jul. 2014.

[8] C. Arnold, J. Parlebas, R. Meiser, and T. Zwick, "Fully reconfigurable manifold multiplexer," *IEEE Trans. Microw. Theory Techn.*, vol. 65, no. 10, pp. 3885–3891, Oct. 2017.

[9] B. Yassini, M. Yu, D. Smith, and S. Kellett, "A *Ku*-band high-*Q* tunable filter with stable tuning response," *IEEE Trans. Microw. Theory Techn.*, vol. 57, no. 12, pp. 2948–2957, Dec. 2009.

[10] S. Nam, B. Lee, C. Kwak, and J. Lee, "Contactless tuning plunger and its application to K-band frequency-tunable cavity filter," *IEEE Trans. Microw. Theory Techn.*, vol. 67, no. 7, pp. 2713–2719, Jul. 2019.

[11] L. Pelliccia, F. Cacciamani, P. Farinelli, and R. Sorrentino, "High-*Q* tunable waveguide filters using ohmic RF MEMS switches," *IEEE Trans. Microw. Theory Techn.*, vol. 63, no. 10, pp. 3381–3390, Oct. 2015.

[12] U. Rosenberg, R. Beyer, P. Krauß, T. Sieverding, A. Papanastasiou, M. Pueyo-Tolosa, P. M. Iglesias, and C. Ernst, "Novel remote controlled dual mode filter providing flexible re-allocation of center frequency and bandwidth," in *IEEE MTT-S Int. Microw. Symp. Dig.*, May 2016, pp. 1–3.

[13] A. Périgaud, O. Tantot, N. Delhote, S. Verdeyme, S. Bila, D. Pacaud, L. Carpentier, J. Puech, L. Lapierre, and G. Carayon, "Continuously tuned Ku-band cavity filter based on dielectric perturbers made by ceramic additive manufacturing for space applications," *Proc. IEEE*, vol. 105, no. 4, pp. 677–687, Apr. 2017.

[14] S. Nam, B. Lee, C. Kwak, and J. Lee, "A new class of K-band high-Q frequency-tunable circular cavity filter," *IEEE Trans. Microw. Theory Techn.*, vol. 66, no. 3, pp. 1228–1237, Mar. 2018.

[15] F. Huang and R. R. Mansour, "Tunable compact dielectric resonator filters," in *Proc. Eur. Microw. Conf. (EuMC)*, Oct. 2009, pp. 559–562.

[16] W. Dong Yan and R. R. Mansour, "Tunable dielectric resonator bandpass filter with embedded MEMS tuning elements," *IEEE Trans. Microw. Theory Techn.*, vol. 55, no. 1, pp. 154–160, Jan. 2007.

[17] S. Fouladi, F. Huang, W. D. Yan, and R. R. Mansour, "High-Q narrowband tunable combline bandpass filters using MEMS capacitor banks and piezomotors," *IEEE Trans. Microw. Theory Techn.*, vol. 61, no. 1, pp. 393–402, Jan. 2013.

[18] A. F. Azarnaminy and R. Mansour, "A combline tunable filter with loss compensation circuit," in *IEEE MTT-S Int. Microw. Symp. Dig.*, Jun. 2018, pp. 1367–1369.

[19] F. Huang, S. Fouladi, and R. R. Mansour, "High-*Q* tunable dielectric resonator filters using MEMS technology," *IEEE Trans. Microw. Theory Techn.*, vol. 59, no. 12, pp. 3401–3409, Dec. 2011.

[20] J.-X. Xu, L. Yang, Y. Yang, and X. Y. Zhang, "High-*Q*-factor tunable bandpass filter with constant absolute bandwidth and wide tuning range based on coaxial resonators," *IEEE Trans. Microw. Theory Techn.*, vol. 67, no. 10, pp. 4186–4195, Oct. 2019.

[21] J. C. Melgarejo, J. Ossorio, S. Cogollos, M. Guglielmi, V. E. Boria, and J. W. Bandler, "On space mapping techniques for microwave filter tuning," *IEEE Trans. Microw. Theory Techn.*, vol. 67, no. 12, pp. 4860–4870, Dec. 2019.

[22] J. Ossorio, J. Vague, V. E. Boria, and M. Guglielmi, "Exploring the tuning range of channel filters for satellite applications using electromagnetic-based computer aided design tools," *IEEE Trans. Microw. Theory Techn.*, vol. 66, no. 2, pp. 717–725, Feb. 2018.

[23] C. Kwak, M. Uhm, and I. Yom, "Feasibility study on combline filter for tunable filters," in *Proc. Asia–Pacific Microw. Conf. (APMC)*, Nov. 2013, pp. 927–929.

[24] J. S. Parish, N. Somjit, and I. C. Hunter, "Continuous frequency and bandwidth tunable combline cavity bandpass filters with internally mounted motors," *IET Microw., Antennas Propag.*, vol. 12, no. 15, pp. 2332–2337, Dec. 2018.

[25] E. Doumanis, G. Goussetis, J. Vuorio, K. Hautio, O. Amper, E. Kuusmik, and J. Pallonen, "Tunable filters for agile 5G new radio base transceiver stations," *IEEE Microw. Mag.*, vol. 22, no. 11, pp. 26–37, Nov. 2021.

[26] G. Basavarajappa and R. R. Mansour, "Design methodology of a tunable waveguide filter with a constant absolute bandwidth using a single tuning element," *IEEE Trans. Microw. Theory Techn.*, vol. 66, no. 12, pp. 5632–5639, Dec. 2018.

[27] R. R. Mansour, "A tunable quarter-wavelength coaxial filter with constant absolute bandwidth using a single tuning element," *IEEE Microw. Wireless Compon. Lett.*, vol. 31, no. 6, pp. 658–661, Jun. 2021.

[28] J. Ossorio, V. E. Boria, and M. Guglielmi, "Dielectric tuning screws for microwave filters applications," in *IEEE MTT-S Int. Microw. Symp. Dig.*, Jun. 2018, pp. 1253–1256.

[29] G. Macchiarella, L. Accatino, and A. Malagoli, "Design of Ka-band tunable filters in rectangular waveguide with constant bandwidth," in *Proc. IEEE Asia–Pacific Microw. Conf. (APMC)*, Dec. 2020, pp. 622–624.

[30] A. Sharma, J. Ossorio, D. Smacchia, T. Tronser, S. Cogollos, V. E. Boria, and M. Guglielmi, "Remote reconfiguration of microwave filters using dielectric tuners," *IEEE Trans. Microw. Theory Techn.*, vol. 71, no. 7, pp. 3051–3064, Jul. 2023.

[31] M. Hoeft, A. Kronberger, and O. Bartz, "Tunable bandpass filters for multi-standard applications," in *Proc. German Microw. Conf.*, Mar. 2008, pp. 1–4.

[32] R. Beyer, S. Heisen, and U. Rosenberg, "CAD of conductor loaded cavity filters with wide band tuning capability," in *Proc. 32nd Eur. Microw. Conf.*, Sep. 2002, pp. 1–4.

[33] A. Sharma, S. Cogollos, V. E. Boria, and M. Guglielmi, "Analysis and design of re-configurable combline filters using dielectric tuners," in *Proc. 51st Eur. Microw. Conf. (EuMC)*, Apr. 2022, pp. 1–12.

[34] M. El Sabbagh, K. A. Zaki, H.-W. Yao, and M. Yu, "Full-wave analysis of coupling between combline resonators and its application to combline filters with canonical configurations," *IEEE Trans. Microw. Theory Techn.*, vol. 49, no. 12, pp. 2384–2393, Dec. 2001.

[35] Y. Xie, F.-C. Chen, and Q.-X. Chu, "Tunable cavity filter and diplexer using in-line dual-post resonators," *IEEE Trans. Microw. Theory Techn.*, vol. 70, no. 6, pp. 3188–3199, Jun. 2022.

[36] A. Widaa, C. Bartlett, and M. Höft, "Tunable coaxial bandpass filters based on inset resonators," *IEEE Trans. Microw. Theory Techn.*, vol. 71, no. 1, pp. 285–295, Jan. 2023.

[37] W. Lin, K. Zhou, and K. Wu, "Band-reconfigurable tunable bandpass filters based on mode-switching concept," *IEEE Trans. Microw. Theory Techn.*, vol. 71, no. 3, pp. 1125–1135, Mar. 2023.

[38] (Dec. 22, 2022). *CST Microwave Studio*. [Online]. Available: https://www.3ds.com/products-services/simulia/products/cst-studiosuite/

[39] J. Ossorio, J. C. Melgarejo, V. E. Boria, M. Guglielmi, and J. W. Bandler, "On the alignment of low-fidelity and high-fidelity simulation spaces for the design of microwave waveguide filters," *IEEE Trans. Microw. Theory Techn.*, vol. 66, no. 12, pp. 5183–5196, Dec. 2018.

[40] P. A. Smith, "Performance of YBCO thick films in high-Q structures," in *Proc. IEE Colloq. Superconducting Microw. Circuits*, 1996, pp. 1–5.

[41] Y. Burachevsky and I. Bakeev, "Properties of electrical insulation coatings from yttrium-stabilized zirconia and alumina," in *Proc. 7th Int. Congr. Energy Fluxes Radiat. Effects (EFRE)*, Sep. 2020, pp. 827–830.

[42] Y. Marchives, N. Delhote, S. Verdeyme, and P. M. Iglesias, "Wide-band dielectric filter at C-band manufactured by stereolithography," in *Proc. 44th Eur. Microw. Conf.*, Oct. 2014, pp. 187–190.

[43] G. L. Matthaei, L. Young, and E. M. T. Jones, *Microwave Filters, Impedance-Matching Networks, and Coupling Structures*. Norwood, MA, USA: Artech House, 1980.

[44] S. Shukla, N. Gomathi, and R. George, "Autocatalytic silver-plating of aluminium radio frequency waveguides with autocatalytic nickel as the undercoat for space applications," *Surf. Topography, Metrology Properties*, vol. 2, no. 4, pp. 1–7, Nov. 2014.

[45] R. Levy and T. E. Rozzi, "Precise design of coaxial low-pass filters," *IEEE Trans. Microw. Theory Techn.*, vol. MTT-16, no. 3, pp. 142–147, Mar. 1968.

[46] E. Sorolla, S. Anza, B. Gimeno, A. M. P. Perez, C. Vicente, J. Gil, F. J. S. Prez, F. D. Quesada, A. Alvarez, and V. E. Boria, "An analytical model to evaluate the radiated power spectrum of a multipactor discharge in a parallel-plate region," *IEEE Trans. Electron Devices*, vol. 55, no. 8, pp. 2252–2258, Aug. 2008.

[47] J. de Lara, F. Perez, M. Alfonseca, L. Galan, I. Montero, E. Roman, and D. R. Garcia-Baquero, "Multipactor prediction for on-board spacecraft RF equipment with the MEST software tool," *IEEE Trans. Plasma Sci.*, vol. 34, no. 2, pp. 476–484, Apr. 2006.
[48] J. Vague, J. C. Melgarejo, M. Guglielmi, V. E. Boria, S. Anza, C. Vicente, M. R. Moreno, M. Taroncher, B. G. Martínez, and D. Raboso, "Multipactor effect characterization of dielectric materials for space applications," *IEEE Trans. Microw. Theory Techn.*, vol. 66, no. 8, pp. 3644–3655, Aug. 2018.
[49] *Multipacting Handbook*, document ECSS-E-HB-20-01A, European Cooperation for Space Standarization (ECSS), ESA-ESTEC, ESA Publication Division, Amsterdam, The Netherlands, Jun. 2020.

ABHISHEK SHARMA (Student Member, IEEE) was born in New Delhi, India, in 1992. He received the bachelor's degree in electronics and communication from the Technical University of Uttar Pradesh, India, in 2014, and the master's degree in microwave and optical communication from the Department of Electronics and Communication, Delhi Technological University (formerly DCE), India, in 2017. He is currently pursuing the Ph.D. degree with the Microwave Applications Group (GAM-ITEAM), Universitat Politècnica de València (UPV), Valencia, Spain, like an Early Stage Researcher of the TESLA Network.

From 2017 to 2019, he was an RF Design Engineer with the Microwave Component Division of Bharat Electronics Ltd., under the Ministry of Defence, India, where he participated in the design of TR modules for active phased arrays and radars. During the Ph.D. studies, he developed novel compact solutions for reconfigurable waveguide filters and multiplexers. His research interests include high-power filter design, reconfigurable filters, transmit-receive modules, and RF subsystems and radars.

SANTIAGO COGOLLOS (Member, IEEE) was born in Valencia, Spain, in 1972. He received the "Ingeniero Superior de Telecomunicación" and "Doctor Ingeniero de Telecomunicación" degrees from Universitat Politècnica de València (UPV), Valencia, in 1996 and 2002, respectively.

In 2000, he joined the Communications Department, UPV, where he was an Assistant Lecturer, from 2000 to 2001; a Lecturer, from 2001 to 2002; an Associate Professor, from 2002 to 2022; and became a Full Professor, in 2022. He has collaborated with the European Space Research and Technology Centre of the European Space Agency in the development of modal analysis tools for payload systems in satellites. In 2005, he held a postdoctoral research position involved in the area of new synthesis techniques in filter design with the University of Waterloo, Waterloo, ON, Canada. His research interests include applied electromagnetics, mathematical methods for electromagnetic theory, analytical and numerical methods for the analysis of microwave structures, and the design of waveguide components for space applications.

VICENTE E. BORIA (Fellow, IEEE) was born in Valencia, Spain, in May 1970. He received the Ingeniero de Telecomunicacin (Hons.) and Doctor Ingeniero de Telecomunicacin degrees from the Universidad Politècnica de València (UPV), Valencia, in 1993 and 1997, respectively. In 1993, he joined the Departamento de Comunicaciones, UPV, where he has been a Full Professor, since 2003. In 1995 and 1996, he was a Spanish Trainee with the European Space Research and Technology Centre, European Space Agency (ESTEC-ESA), Noordwijk, The Netherlands, where he was involved in the area of EM analysis and design of passive waveguide devices. He has authored or coauthored ten chapters in technical textbooks, 200 papers in refereed international technical journals, and more than 250 papers in international conference proceedings. His current research interests include the analysis and automated design of passive components, left-handed and periodic structures, and the simulation and measurement of power effects in passive waveguide systems. He has been a member of the IEEE Microwave Theory and Techniques Society (IEEE MTT-S) and the IEEE Antennas and Propagation Society (IEEE AP-S) since 1992. He is also a member of the European Microwave Association (EuMA) and the Technical Committees of the IEEE-MTT International Microwave Symposium and the European Microwave Conference. He serves as an Editorial Board Member of the *International Journal of RF and Microwave Computer-Aided Engineering*. He has been the Chair for the 48th European Microwave Conference held in Madrid, Spain. He acts as a regular reviewer for the most relevant IEEE and IET technical journals on the areas of interest. He was an Associate Editor of the IEEE MICROWAVE AND WIRELESS COMPONENTS LETTERS from 2013 to 2018 and the *IET of Electronics Letters* from 2015 to 2018. He serves as a Subject Editor for *Microwave Journal* and the *IET of Electronics Letters*.

MARCO GUGLIELMI (Life Fellow, IEEE) was born in Rome, Italy, in December 1954. He received the "Laurea in Ingegneria Elettronica" degree from the University of Rome "La Sapienza," Rome, in 1979, the M.S. degree in engineering from the University of Bridgeport, Bridgeport, CT, USA, in 1982, and the Ph.D. degree in electrophysics from Polytechnic University, Brooklyn, NY, USA, in 1986. He also attended the Scuola di Specializzazione in Elettromagnetismo Applicato, University of Rome "La Sapienza," in 1980. From 1984 to 1986, he was an Academic Associate with Polytechnic University, where he was an Assistant Professor, from 1986 to 1988. From 1988 to 1989, he was an Assistant Professor at the New Jersey Institute of Technology, Newark, NJ, USA. In 1989, he joined the RF System Division, European Space Agency, European Space Research and Technology Centre (ESTEC), Noordwijk, The Netherlands, as a Senior Microwave Engineer, where he was in charge of the development of microwave filters and electromagnetic simulation tools. In 2001, he was appointed as the Head of the Technology Strategy Section, ESTEC, where he contributed to the development of management processes and tools for the formulation of a European Strategy for Space Technology Research and Development. In 1981, he was awarded a Fulbright Scholarship in Rome and a Halsey International Scholarship Program (HISP) from the University of Bridgeport. In 2014, he retired from the European Space Agency and is currently an Invited Senior Researcher at the Universidad Politècnica de València (UPV), Valencia, Spain. He has been elevated to the grade of a fellow of the IEEE "For Contributions to Multimode Equivalent Networks and Microwave Filter Design," in January 2013.